Typology of defects in DEMO divertor target mockups.

Y. Addab[1], M. Richou[1],*, M. Ramaniraka[1], N. Vignal[1], E. Visca[2], G. Dose[2], S. Roccella[2], H. Greuner[3], M. Missirlian[1] and J.H. You[3]

[1] CEA, IRFM, F-13108, Saint-Paul-Lez-Durance, France
[2] ENEA, Department of Fusion and Technology for Nuclear Safety and Security, via E. Fermi 45, 00044 Frascati, Italy
[3] Max Planck Institute for Plasma Physics, Boltzmann Str. 2, 85748 Garching, Germany

E-mail: marianne.richou@cea.fr

Abstract

We analyzed data from ultrasonic testing and infrared thermography non-destructive examinations performed on a subset of 25 small scale water-cooled target mockups of four target designs developed in the 2nd R&D phase of WPDIV. Examinations were performed before high heat flux tests for the 25 mockups and after high heat flux tests for 18 of them. The detected manufacturing defects are various in size and location. Widths of defects range from 0.2 to 12 mm, which is the entire block width. Angular sizes of defects range from few degrees to 360°. Defects having an angular size less than 50° or a width less than 4 mm are likely to be missed by infrared thermography examinations. After high heat flux tests at 20 MW/m² up to 500 cycles, we noticed no significant evolution of pre-existing defects.

Keywords: Divertor, Target, DEMO, Qualification, Ultrasonic testing, Infrared thermography.

1. Introduction

The divertor target plays a key role: the extraction of heat and particles produced by the fusion reaction [1]. In the DEMO strike point region, we expect thermal loads reaching 10 MW/m² during normal operations (2 h pulses) and thermal loads to 20 - 40 MW/m² in case of slow transient events [2, 3, 4]. Central disruptions (~1 GJ/m², ~10 ms) could also occur in DEMO reactor [5]. All these elements make heat extraction being a major technological challenge. The eventual presence of defects in divertor plasma facing components (PFCs) could drastically decrease their heat exhaust capability and their lifetime. Defects in PFCs can be materials intrinsic defects (porosities, inclusions, cracks, …) or defects linked to joining process. Moreover damages can be initiated during plasma operation [6] and phenomena such as cracking [5], plastic fatigue [6], corrosion of the cooling pipe [7], materials embrittlement due to neutron irradiation [8, 9, and 10], are likely to occur. The origin and type of possible defects in PFCs are various and their evolution under plasma operation is not well known. It appears as necessary to define a qualification procedure and associated defect acceptance criteria in order to ensure the quality of these critical components before mounting on the reactor. The present work is led in the framework of the work package 'Divertor' (WPDIV) of the EUROfusion Consortium which aims at developing design concepts and technologies of the divertor target for the European DEMO [11]. We analyzed data from ultrasonic testing and infrared (IR) thermography nondestructive examinations (NDEs) performed on a subset of 25 small scale water-cooled target mockups developed in the 2nd R&D phase of WPDIV. We analyzed four target designs of tungsten mono-block type with a copper-base cooling pipe, which were submitted to high heat flux tests. NDEs were performed before high heat flux tests for all mockups and after high heat flux tests for 18 of them. In this paper we study the typology of defects (size, location) detected after fabrication, and their evolution due to high heat flux tests performed at 20 MW/m².

2. Experimental part

2.1 Mock-ups description

We analyzed data from a subset of 25 mockups (100 blocks), from four target designs. Table 1 describes mockups specificities and details the number of analyzed mockups, further details on the different concepts are given in [12]. All mockups were of tungsten mono-block type with a copper-base cooling pipe. ITER-like target design consists of W block joined with a CuCrZr cooling pipe with a Cu interlayer in between (Cu thicknesses : 100 µm, 300 µm and 1 mm). ITER-like mockups were joined by hot radial pressure (HRP). Composite target design consists of W blocks joined together with a W wire-reinforced Cu composite pipe. Composite mockups were joined by brazing. Functionally graded material (FGM) target design consists of W block joined with a CuCrZr cooling pipe with a W/Cu graded interlayer (FGM interlayer thicknesses : 25 µm, 500 µm). FGM mockups were joined by hot isostatic pressure (HIP) [13]. Two mockups having a thin 20 µm Cu interlayer were also joined by HIP. Thermal break target design consists of W block joined with a CuCrZr cooling pipe with a 1.5 mm Cu interlayer in between. The interlayer is notched in the flux facing region. Thermal break mockups were joined by brazing. The ITER-like target design (together with the HRP technology) has been selected for the conceptual design phase and, the composite pipe target design was endorsed for further technology R&D [12]. All design concepts passed with success the specified design criterion (500 pulses at 20 MW/m ²with a hot coolant of 130 °C) [12].

Mockup Specificity	**Joining technique**	**Qty**	**Tested at ≥ 20 MW/m²**
20 µm Cu interlayer (FGM)	Hot Isostatic Pressure	2	1/2
25 µm FGM interlayer (FGM)		4	2/4
500 µm FGM interlayer (FGM)		3	2/3
100 µm Cu interlayer (ITER-like)	Hot Radial Pressure	2	1/2
300 µm Cu interlayer (ITER-like)		2	2/2
1 mm Cu interlayer, W supplier: AT&M (ITER-like)		3	2/3
1 mm Cu interlayer, W supplier: ALMT (ITER-like)		2	2/3
Wf/Cu pipe (composite)	Brazing	3	2/3
Cu thermal break interlayer (thermal break)	Brazing	4	3/4

Table 1 - Mockups specificities and number of considered mockups. 25 mockups in total. (Qty means quantity).

2.2 IR thermography

We performed IR thermography examinations on SATIR facility [14]. Mockups are submitted to a thermal solicitation via the circulating water in order to evaluate their heat exhaust capability, and thus to check the existence of defects in mockups. SATIR facility has two pressurized independent water injection lines (hot and cold water) synchronized by an industrial programmable controller. In the examinations presented here, inlet water pressure was set at 10 bars and flow rate was set at 4 m^3h^{-1}. During testing, mockups are first heated up to 100°C ± 5°C (by injecting hot water). Once thermal equilibrium is reached, the mockups are cooled down to 13°C ± 3°C in a few ms via the second water injection line. A CEDIP JADE II (λ= 3-5 µm) infrared camera equipped with a 50 mm lens records the thermal response of the mockups. We evaluate the mockup heat exhaust capability by comparing surfaces cooling dynamics of the tested mockups and of reference ones, supposed free of defects. We call "DTref" the difference between the temperature of the tested mockup surface and the temperature of the reference mockup surface. We call DTrefmax the maximum of DTref over the thermal sollicitation. A DTrefmax value higher than 8°C indicates the existence of a defect [15]. After post-treatment, a DTrefmax map is represented for each analyzed mockup face. SATIR examinations were performed on all mockup faces (front, left, back and right face). In DTref maps, pixels size is about 0.5 x 0.5 mm².

2.3 Ultrasonic testing

UT was performed at the laboratories of ENEA Frascati. This facility was widely used for the systematic examinations of all the mockups manufactured in the framework of the development of DEMO divertor target [16]. Pulse-echo water gap technique was used to characterize the mockups. The tests are conducted by inserting an ultrasonic pulser/receiver probe inside the CuCrZr tube, which is beforehand filled with distilled water. A two-degree-of-freedom translational and rotational system make the probe move along the mockups. During an acquisition, the mockup is positioned vertically. The probe is inserted in the CuCrZr tube from the top and goes down while acquiring echo signals. Once arrived at the bottom of the mockup it comes back to its initial position (on top) and rotates by 1 degree before going down again (and so on). The test finishes after a rotation of 360°. The axial step is 80 µm; the angular step is 1°. The diameter of the piezoelectric crystal inside the probe is 3 mm, and it works at a nominal frequency of 15 MHz.

2.4 High heat flux tests in GLADIS

HHF tests were carried out in the HHF test facility GLADIS at IPP Garching [17]. The aim of the HHF tests was the evaluation of the different concepts, the experimental validation of numerical predicted thermo-mechanical

behaviour under DEMO relevant heat load and cooling and finally the identification of the most promising concept. As "initial quality assessment" after manufacturing, the following tests with cold water, low pressure (20 °C inlet, 1 MPa static pressure, 12 m/s axial velocity, 10 s loading) were performed for each mock-up:

- Screening from 6 to 25 MW/m², 5 cycles each step,
- 100 cycles at 10 MW/m² as low cycle test.

After having passed this assessment without damage further tests like cyclic hot water high pressure or cold-water high power (20 MW/m²) were performed as described in the literature [18]. The applied hydrogen neutral beam (150 mm FWHM) ensures a simultaneous and homogeneous heating of the mock-ups. The comparison between the calorimetrically measured absorbed power and the calculated incident power is in an agreement within ±5%. The central surface temperature of the exposed mock-ups was measured with one- and two-colour pyrometers as well as monitored by an infrared camera Infratec VARIOCAM HD.

2.5 Defects sizing and location

Interfaces are preferred place for defects to occur and develop, and most of the defects were detected at interfaces. In the following, defects detected by IR thermography and/or UT are identified by an angular position θ, an angular size Δθ, and a width Δx (defect length along the cooling tube). The origin of θ is in the middle of the flux facing face, as illustrated in Figure 1. In this paper, we deal with bonding defects at the W-Cu interface, or at the Cu-pipe interface.

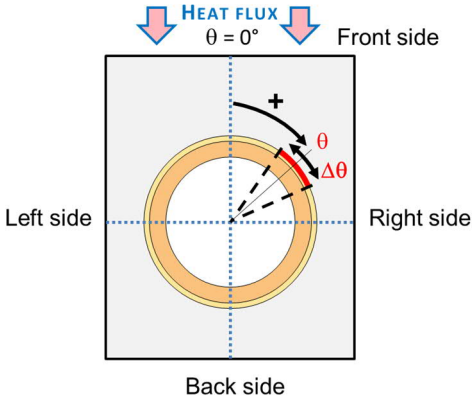

Figure 1 - Convention of sizing and localization for defects measurements

We classify the positions of defects in 4 classes, linked to the faces of a block: front side for θ∈]-45;45[, left side for θ∈]-135;-45[, right side for θ∈]45;135[, and back side for |θ| > 135°. The reported angular size can belong either to a continuous defect or to a global defective zone (discontinuous defect). The width of defects is measured only by UT.

The most disturbing defects regarding high heat flux tests are the closest to the heat flux, in other words the closest to front part of blocks. Because of their location, these defects are likely to cause overheatings. The less disturbing defects are those located at the backside of blocks.

The detection of defects does not necessarily imply a decrease in the heat extraction capability, which is assessed while performing high heat flux tests.

3. Results

3.1 Typology of defects

Figure 2 presents widths and angular sizes of the 57 defects detected on the considered subset of 25 mockups by both IR thermography and UT (bold black edges) and of defects detected only by UT (colored edges).

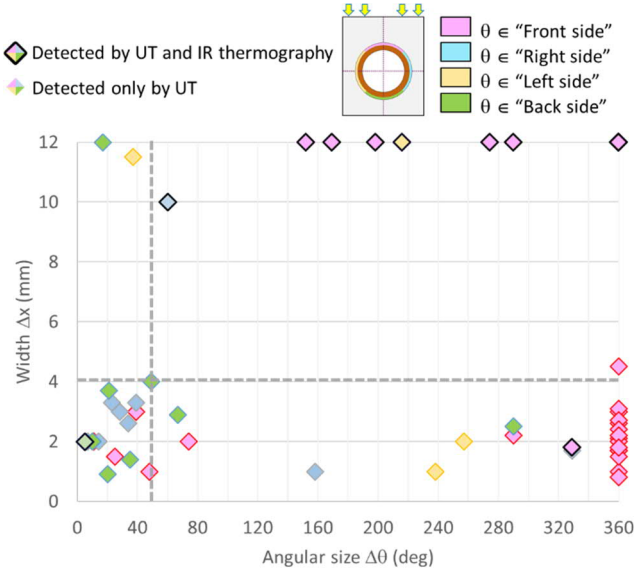

Figure 2 Widths and angular sizes of defects detected before HHFT by both infrared thermography and ultrasonic testing (bold black edges) and of defects detected only by ultrasonic testing (colored edges).The dashed lines represent the Δx and Δθ values (4 mm, 50°) below which defects are likely to be detected only by UT. The color code indicates ranges of defects location. Pink : front side θ ∈]-45°;45°[, yellow : left side θ ∈]-135°;-45°[, blue : right side θ ∈]45°;135°[, and green: backside |θ| > 135°.

First, this plot shows that the ranges of widths and angular sizes of defects are wide. Widths range from 0.2 to 12 mm, which is the entire block width. Angular sizes range from few degrees to 360°, meaning that defect is all around the tube.

The range of defect locations is also wide and we noticed no preferred locations for defects. Note that the location of circumferential defects was set arbitrarily to 0°. From these results it appears that the manufacturing defects are various in size and location. 60% of defects have an angular size higher than 50° and 23% of defects have a width higher than 6 mm (half of a block depth). Besides, we can note that there is a lack of data in the width range 4 mm - 9 mm. It is not clear for the moment if it is due to a lack of statistics or if there were a physical reason for that, increasing statistics would help. Measuring defects in this empty region could also be helpful to rule on detectability and on behavior of defects under high heat flux tests. Based on the analysis of the population of detected defects, the vertical and horizontal dashed lines in Figure 2 represent the Δx and $\Delta\theta$ values of 4 mm and 50° below which defects are likely to be detected only by UT (which have a higher sensitivity). The number of defects detected by UT is about three times higher than the number of defects detected by IR thermography.

3.2 High heat flux tests

The most disturbing defects regarding the handling capability under high heat flux tests are the ones located at the top-right part of Figure 2. They are centered near the front face of mockups, they have a width of 12 mm (entire block depth) and a large angular size, higher than 150°.

Figure 3 shows IR images of two mockups after 100 pulses at 10 MW/m² (moderate conditions).

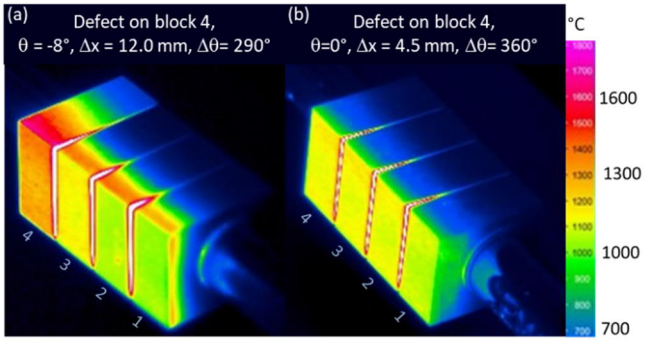

Figure 3 Infrared images of mockups after 100 pulses at 10 MW/m² (a) IR image of a mockup presenting a 12 mm width defect on block 4 (b) IR image of a mockup presenting a 4.5 mm defect on block 4.

Figure 3 (a) shows a non-uniform thermal response due to the presence in this mockup of a defect centred on the front side of block 4 and having an angular size of 290°, spreading through the entire block depth (12 mm). The group of mockups presenting the disturbing defects mentioned above showed similar non-uniform thermal responses at moderate flux of 10 MW/m² and were not tested at 20 MW/m². It is worth to underline that all these defects, which induced non-uniform thermal responses were detected by SATIR. Figure 3 (b) shows a uniform thermal response of the tested mockup despite the presence on block 4 of a defect having an angular size of 360° and a width of 4.5 mm. Mockups showing similar uniform thermal responses were tested at higher flux conditions.

Figure 4 presents the widths and angular sizes of the 39 defects detected by UT on the subset of 18 mockups (72 blocks) that were tested at 20 MW/m². The defects identified in this graph are the same as before HHFT (see Figure 2) except for seven of them - all detected on 100 µm Cu interlayer mockups (not retained concept) - which increased in width by between 1 and 3 mm. Those seven defects have an angular size higher than 320°. It is not yet clear if we should talk about an evolution of defects or about a creation of defects near pre-existing ones. Extra-investigations are currently performed in order to clarify this point. In all other considered cases the size of defects did not change after HHFT.

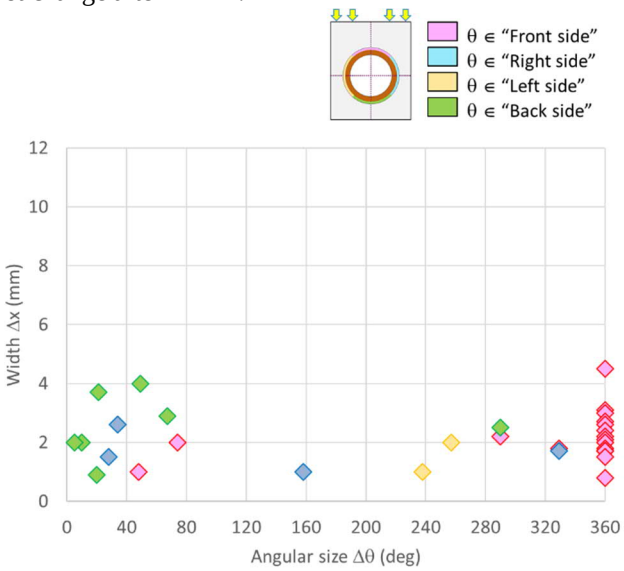

Figure 4 Widths and angular sizes of defects detected by UT on mockups that were tested at 20 MW/m².

4. Conclusions

In this work, 25 mockups of 4 target design concepts were analyzed by IR thermography and UT. We found that after fabrication, defects had a wide range of sizes and locations. We noticed a lack of data in the width range of 4 mm - 9 mm. In the future, analyzing mock-ups with such defects could be helpful to rule on non-destructive techniques detectability and on the impact of such defects on the thermal behavior under high heat flux tests. Defects detected using IR thermography have $\Delta\theta$ >50° or Δx > 4 mm. Those defects impacted the mockups thermal response under high heat flux tests at 10 MW/m² and were consequently not tested at 20 MW/m². Mockups tested at 20 MW/m² (500 cycles), showed no significant evolution of pre-existing defects.

Acknowledgements

This work has been carried out within the framework of the EUROfusion Consortium and has received funding from the Euratom research and training programme 2014-2018 and 2019-2020 under grant agreement No 633053. The views and opinions expressed herein do not necessarily reflect those of the European Commission.

References

[1] Turnyanskiy M, Neu R, Albanese R, Ambrosino R, Bachmann C, Brezinsek S, Donne T, Eich T, Falchetto G, Federici G, Kalupin D, Litaudon X, Mayoral ML, McDonald DC, Reimerdes H, Romanelli F, Wenninger R and You JH 2015 *Fusion Engineering And Design* **96-97** 361–364

[2] Pitts RA, Bonnin X, Escourbiac F, Frerichs H, Gunn JP, Hirai T, Kukushkin AS, Kaveeva E, Miller MA, Moulton D, Rozhansky V, Senichenkov I, Sytova E, Schmitz O, Stangeby PC, De Temmerman G, Veselova I and Wiesen S 2019 *Nuclear Materials and Energy* **20** 100696

[3] Asakura N, Hoshino K, Utoh H, Someya Y, Suzuki S, Bachmann C, Reimerdes H, Wenninger R, Kudo H, Tokunaga S, Homma Y, Sakamoto Y, Hiwatari R, Tobita K, You JH, Federici G, Ezato K, Seki Y, Ueda Y and Ohno N 2018 *Fusion Engineering And Design* **136** 1214–1220

[4] Maviglia F, Federici G, Strohmayer G, Wenninger R, Bachmann C, Albanese R, Ambrosino R, Li M, Loschiavo VP, You JH and Zani L 2016 *Fusion Engineering And Design* **109** 1067–1071

[5] Bachmann C, Plant description document, *EUROfusion report*: 2KVWQZ, 2020.

[6] Loewenhoff T, Burger A, Linke J, Pintsuk G, Schmidt A, Singheiser L and Thomser C 2011 Physica Scripta **T 145** 014057

[7] Obitz C, Öijerholm J, Wikman S and Bratu E 2016 *Nuclear Materials and Energy* **9** 261–266.

[8] Klimenkov M, Jantsch U, Rieth M, Schneider HC, Armstrong DEJ, Gibson J and Roberts SG 2016 *Nuclear Materials and Energy* **9** 480-483.

[9] Noce S, Dose G, Flammini D, Imbriani V, Mazzone G, Moro F, Roccella S, Romanelli F, Villari R, Visca E and You JH 2020 *Fusion Engineering And Design* **155** 111730

[10] You JH, Villari R, Flammini D, Marzullo D and Mazzone G 2020 *Nuclear Materials and Energy* **23** 100745

[11] You JH, Visca E, Barrett T, Boswirth B, Crescenzi F, Domptail F, Fursdon M, Gallay F, Ghidersae BE, Greunera H, Li M, Muller AV, Reiser J, Richou M, Roccella S and Vorpahl C 2018 *Nuclear Materials and Energy* **16** 1-11

[12] You JH, Visca E, Barrett T, Boswirth B, Crescenzi F, Domptail F, Dose G, Fursdon M, Gallay F, Greuner H, Hunger K, Lukenskas A, Muller AV, Richou M, Roccella S, Vorpahl C and Zhang K 2021 *Journal of Nuclear Materials* **544** 152670

[13] Richou M, Gallay F, Boswirth B, Chu I, Dose G, Greuner H, Kermouche G, Lenci M, Loewenhoff T, Maestracci R, Meillot E, Missirlian M, Pastor JY, Quet A, Roccella S, Tejado E, Wirtz M, Visca E, Pintsuk G and You JH 2020 *Fusion Engineering And Design* **157** 111610

[14] Vignal N, Desgranges C, Cantone V, Richou M, Courtois X, Missirlian M and Magaud P 2013 *Fusion Engineering And Design* **88** 1818– 1822

[15] Gallay F, Richou M, Vignal N, Lenci M, Roccella S, Kermouche G, Visca E and You JH 2017 *Physica Scripta* **T170** 14015

[16] Roccella S, Reale A, Tati A, Visca E, Palermo M and Gavila P 2019 *Fusion Engineering And Design* **146** 2356–2360

[17] Greuner H, Boeswirth B, Boscary J and McNeely P 2007 *Journal of Nuclear Materials* **367** 1444-1448

[18] Greuner H, Boswirth B, Barrett TR, Crescenzi F, Gallay F, Hunger K, Richou M, Visca E, von Muller A and You JH 2019 *Fusion Engineering And Design* **146** 216–219